Colloid Polym Sci (2015) 293:1695–1703
DOI 10.1007/s00396-015-3553-4

ORIGINAL CONTRIBUTION

Reverse microemulsion-mediated synthesis of Au@SiO_2 hybrid nanoparticles with different morphologies

Yingjie Ren · Xia Xin · Weiyue Tang · Yongjie Zhang · Jinglin Shen · Lin Wang

Received: 1 December 2014 / Revised: 28 February 2015 / Accepted: 1 March 2015 / Published online: 15 March 2015

Abstract In this study, we report a simple synthesis of multiple Au nanodots core-silica shell nanoparticles (multi-Au@SiO_2 NPs). The Au@SiO_2 hybrid nanoparticles were synthesized in a water-in-oil microemulsion with a composition of polyoxyethylene(10) tertoctylphenyl ether (Triton X-100)/1-hexanol/cyclohexane/H_2O and have been fully characterized by transmission electron microscopy (TEM), high-resolution TEM (HR-TEM) observations, X-ray diffraction (XRD), X-ray photoelectron spectroscopy (XPS), Fourier transform infrared (FTIR), UV-vis measurements, and thermogravimetric analysis (TGA). The morphologies of the hybrid nanoparticles of Au@SiO_2 can be easily tuned by the molar ratio of $HAuCl_4$ to $NaBH_4$ and the volume ratio of $HAuCl_4$ aqueous solution to TEOS. As the morphologies of Au@SiO_2 nanoparticles varied, the optical properties also changed as revealed by UV absorption spectrum. These Au@SiO_2 hybrid nanoparticles which possess these properties make them fascinating candidates for a variety of applications such as catalysis and life science.

Keywords Gold · Silica · Nanoparticles · Microemulsion · Morphologies

Y. Ren · X. Xin
National Engineering Technology Research Center for Colloidal Materials, Shandong University, Jinan 250100, People's Republic of China

Y. Ren · X. Xin (✉) · J. Shen · L. Wang
Key Laboratory of Colloid and Interface Chemistry, Ministry of Education, Shandong University, Jinan 250100, People's Republic of China
e-mail: xinx@sdu.edu.cn

Y. Ren · W. Tang · Y. Zhang
China Research Institute of Daily Chemical Industry, Taiyuan, Shanxi 030001, People's Republic of China

Introduction

In recent years, the study of synthesis and assembly of nanoparticles with controlled sizes and shapes received great attention, because the properties of such materials and their potential applications are highly dependent on their structural features [1–4]. For example, gold nanoparticles (Au NP) have received much attention in recent decades due to their physical properties, including electrochemical, catalytic, electromagnetic and colorimetric properties, which are quite distinct from bulk and atomic gold [5, 6]. It is generally accepted that as the size of a material becomes smaller, a variety of new properties will occur.

In order to get gold nanoparticles, hybrid nanomaterials where gold nanoparticles are protected by the outer and/or surrounding media have drawn considerable attention [7–10]. One useful technique for assembling Au nanoparticles is to surround them with a material such as silica (SiO_2) [11]. First of all, SiO_2 is hydrophilic and negatively charged, which can prevent the aggregation of the colloidal particles. Additionally, the surface of the silica layer, which is known to be porous, biocompatible, and nontoxic, can be easily modified using simple techniques, allowing nanoparticles with modified silica shells to be used in various bioapplications [12]. Thus, SiO_2 is considered as an ideal and low-cost material that has already been used for not only coating on Au nanoparticles but also on metal colloids (e.g., Ag) [13], magnetic particles (e.g., Fe_3O_4) [14], semiconductor nanocrystals (e.g., CdTe) [15], and polymers (e.g., polystyrene) [16, 17].

Extensive studies have been performed on the homogeneous coating of metal nanoparticles with silica shells (core–shell particles) [18–24]. Liz-Marzán, Mulvaney, and coworkers have extensively studied metal–silica core–shell particles prepared by a liquid-phase procedure in which the use of a surface primer (a silane coupling agent) was necessary to provide the surface with silanol anchor groups [18–20]. Xia

and co-workers, for instance, prepared silica-coated gold nanospheres [21] and silver nanowires [22] through hydrolysis and condensation of tetraethyl or thosilicate (TEOS) in ethanol. More recently, Graf et al. [23] used poly(vinylpyrrolidone) as a stabilizer to transfer gold and other nanoparticles into ethanol and perform a direct coating with TEOS.

However, an alternative route for coating silica onto Au nanoparticles involves the use of a reverse microemulsion (a water-in-oil (W/O) micellar solution) that allows for the silica coating of small Au nanoparticles (<20 nm) (Scheme 1). The microemulsion method has many advantages such as simplicity of operation, facile controlling of the properties of the hybrid nanoparticles by experimental conditions including the number and size of encapsulated nanocrystals, the core size and shell thickness [25]. Thus, in the present paper, we report a detailed study of $Au@SiO_2$ hybrid nanoparticles synthesized in a water-in-oil microemulsion with a composition of polyoxyethylene(10) tertoctylphenyl ether (Triton X-100)/1-hexanol/cyclohexane/H_2O. The nanoparticles have been fully characterized by a variety of techniques including transmission electron microscopy (TEM), high-resolution TEM (HR-TEM) observations, X-ray diffraction (XRD), X-ray photoelectron spectroscopy (XPS), Fourier transform infrared (FTIR), and UV-vis measurements, as well as thermogravimetric analysis (TGA). It can be indicated that this preparation method can be expanded to a wide range of metals and coating oxides.

Experimental section

Materials

Triton X-100 was purchased from Alfa Aesar, which was treated by a rotary evaporator to remove trace water before use. Tetraethylorthosilicate (TEOS) were obtained from Sigma-Aldrich. Cyclohexane, chlorauric acid ($HAuCl_4$), sodium borohydride ($NaBH_4$), ammonium hydroxide ($NH_3{\cdot}H_2O$) solution (25 wt% in water), and 1-hexanol are from Sinopharm Chemicals. Triple-distilled water was used in all experiments.

Preparation of Au^{3+}-containing water-in-oil microemulsion

In the preparation of Au^{3+}-containing water-in-oil microemulsion, cyclohexane was used as the continuous phase. Pure water or $HAuCl_4$ aqueous solution with a concentration of 0.2 mol L^{-1} was used as the discrete phase. Triton X-100 and 1-hexanol were used as surfactant and co-surfactant, respectively. Typically, 1.25 g Triton X-100 and 0.31 g 1-hexanol were added to 2.35 g cyclohexane to form a stock solution, to which the desired amount of $HAuCl_4$ aqueous solution was added under mechanical stirring (~500 rpm).

Synthesis of $Au@SiO_2$ nanoparticles

In a typical experiment, to the microemulsion mentioned above was added 340-μL aqueous solution of $NaBH_4$ (typically 0.2 mol L^{-1}) under stirring. Stirring was continued while the sample was kept at 26 °C for 0.5 h. Then, 170 μL of diluted $NH_3{\cdot}H_2O$ (14.2 wt%, cal. 3.83 mol L^{-1}) was added under stirring, followed by dropwise addition of 170 μL TEOS 5 min later. The mixture was stirred at 26 °C for another 24 h. After preparation, the as-obtained $Au@SiO_2$ nanoparticles were collected by ultracentrifugation, washed three times by ethanol, and redispersed in ethanol or water under ultrasonication for subsequent characterizations. To tune the final morphology of $Au@SiO_2$ nanoparticles, $n_{(HAuCl4/NaBH4)}$ and $V_{(HAuCl4/TEOS)}$ have been changed by varying the concentration of BH_4^- in the $NaBH_4$ stock solution and the addition volume of $HAuCl_4$ stock solution, respectively. For comparison, we have also prepared SiO_2 nanoparticles. The procedure is the same, but the microemulsion used is without Au^{3+}.

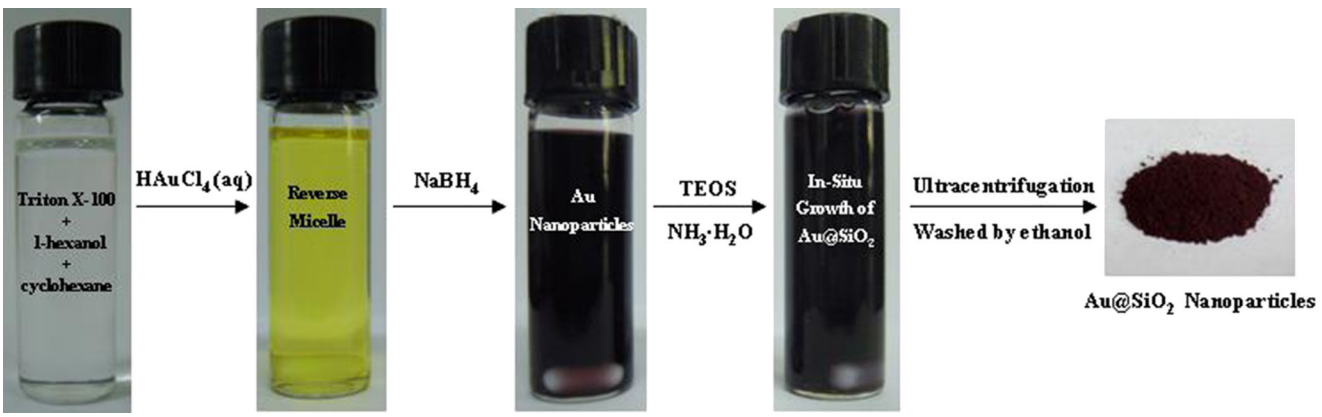

Scheme 1 Synthetic route of $Au@SiO_2$ NPs in a reverse microemulsion

Characterizations

TEM observations were carried out on a JEM 100-CXII with an accelerating voltage of 80 kV. HR-TEM observations were performed on a JEOL-2010 with an accelerating voltage of 200 kV. XRD patterns were collected on a Rigaku D/Max 2200PC diffractometer with a graphite monochrometer and Cu-Kα radiation (λ=0.15418 nm). TGA data were collected using a Universal V3.6 TA Thermal Analysis Q5000 system. The sample was placed in a platinum crucible and heated under a flow of N_2 from ~50 °C to 800 °C at a heating rate of 10 °C min^{-1}. For UV-vis measurements, the nanoparticles were dispersed in ethanol and the spectra were collected on a UV-vis spectrophotometer (Lambda-35, Perkin-Elmer). The powders of Au@SiO_2 nanoparticles were measured on a VERTEX-70/70v FTIR spectrometer (Bruker Optics, Germany).

XPS measurements were performed using a VG Scientific photoelectron spectrometer of ESCALAB-210 using an unmonochromated Al Kα radiation (1486.6 eV) operated at 15 kV, 20 mA under a pressure below 10^{-9} Pa. Survey spectra were recorded in the energy range of 0~1100 eV with a step of 0.4 eV. High-resolution spectra were recorded with a step of 0.1 eV, a dwell time of 100 ms, and a pass energy of 20 eV. A take-off angle of 90° was used in all measurements. The fittings was performed using the AVANTAGE software provided by Thermo Electron at a constant G/L ratio of 0.3±0.05, which describes each component of the complex envelope as a Gaussian-Lorentzian sum function. The background was fitted using a nonlinear Shirley model. Scofield sensitivity factors and measured transmission function were used for quantification. Aromatic carbon C 1 s peak at 284.6 eV was used as reference of binding energy (BE).

Results and discussion

The morphology of Au@SiO_2 nanoparticles with the variations of the volume of $HAuCl_4$

In our experiment, Au@SiO_2 NPs were synthesized through the reduction of Au^{3+} ions (from $HAuCl_4$) during the formation of silica nanoparticles in the reverse microemulsion, which was generated using TX-100 as the surfactant. Figure 1a is the TEM images of pure SiO_2 nanoparticles synthesized in Triton X-100/1-hexanol/cyclohexane/H_2O microemulsion. It can be seen that the SiO_2 particles are uniform and monodisperse. The images clearly show that the reverse microemulsion containing TX-100 led to the effective formation of spherical silica nanoparticles.

Figure 1b, c show the TEM images of the typical samples of the core–shell particles prepared at $n_{(HAuCl4/NaBH4)}$=1 using 0.2 M $HAuCl_4$(aq.), and the volume of $HAuCl_4$ is varied. It is found that with the increase of the amount of $HAuCl_4$, the number of Au points in the core increase gradually.

The analysis of XRD and FTIR results

The wide-angle XRD patterns of nanoparticles with different chemical compositions and structures are summarized in Fig. 2a. The pure SiO_2 nanoparticles only display a halo centered at 2θ=25° (Fig. 2a (a)), indicating the amorphous feature of the particles [26, 27]. For the Au@SiO_2 hybrid nanoparticles (Fig. 2a (c–e)), the obvious diffraction peaks of the Au nanocrystals locate at 38.25°, 44.46°, and 64.69°, respectively, which corresponds to the (111), (200), and (220) planes of metallic Au with a face-centered cubic (fcc) structure (JCPDS no. 65-8601) [28]. It should be noted that the diffraction peak corresponding to the (111) plane is the dominant facet of the Au nanocrystal. XRD result of the bare Au nanocrystals obtained after removal the outer SiO_2 layer of the Au@SiO_2 hybrid nanoparticles by NaOH etching is shown in Fig. 2a (b). It can be seen that after the removal of the SiO_2 layer by NaOH etching, XRD result only remains the patterns of Au nanocrystal and the (111) plane is still the strongest.

For both the pure SiO_2 and Au@SiO_2 nanoparticles, there are two peaks at 1085 and 946 cm^{-1}, which are respectively assigned to the asymmetric stretching vibrations of the Si–O–Si and Si–O(H) bonds form the silica-coating layer [29], and those at 796 and 465 cm^{-1} can be ascribed to the symmetric stretching and bending vibrations of the Si–O–Si bond. Moreover, after removing the outer SiO_2 layer by NaOH etching, the peaks of the asymmetric stretching vibrations of the Si–O–Si and Si–O(H) bonds nearly disappeare and those at 3450 cm^{-1}, which corresponds to the free Si–OH left on the bare Au surfaces, are relatively strong [25]. All of these indicate that the hydrolysis, nucleation, and polycondensation of TEOS occurred successfully, leading to the formation of the SiO_2 networks on the surface of Au nanoparticles.

The analysis of ultraviolet spectrum and thermal stability

It is generally recognized that Au nanoparticles with an average diameter of about 5 nm exhibit surface plasmon resonances (SPRs) in aqueous solution at wavelengths of approximately 520 nm [30–32]. Thus, we attempted to measure the SPRs of the multiple Au nanodots that were encapsulated within the silica nanoparticles. While FTIR preferentially probes the properties of the outer SiO_2 layer, UV measurements mainly detect the optical characteristics of the inner Au nanocrystals. Figure 3 summarizes the absorptions of pure SiO_2 and Au nanocrystals with or without the outer protecting SiO_2 layer. Pure SiO_2 nanoparticles display a continuous increase in the absorption with decreasing wavelength, but no obvious peak could be detected within the investigated

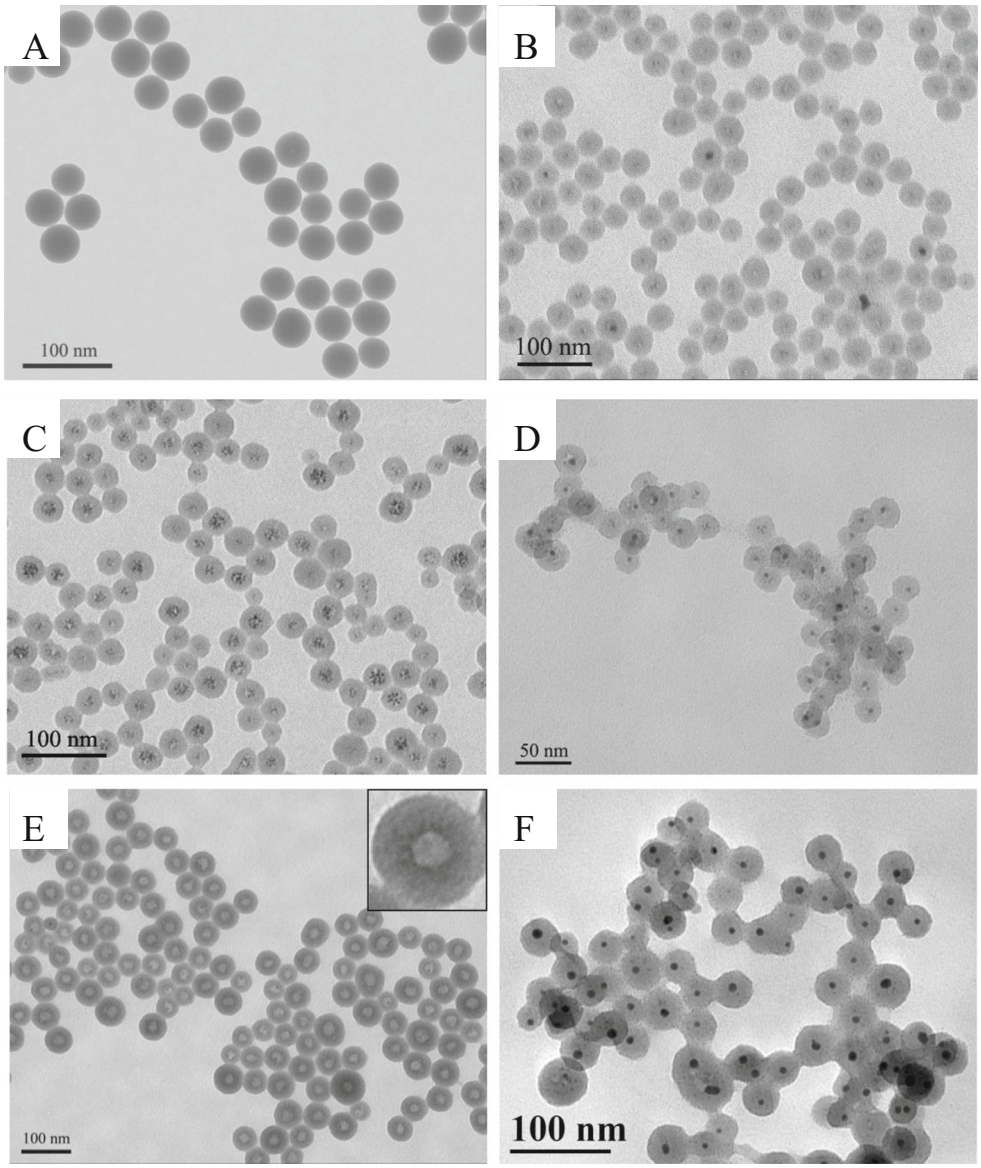

Fig. 1 TEM images of $Au@SiO_2$ NPs that were synthesized using 0.2 M $HAuCl_4$(aq.) obtained at $n_{(HAuCl4/NaBH4)}=1$ and the variations of the volume of $HAuCl_4$ are **a** 0 μL, **b** 100 μL, and **c** 200 μL and using 0.2 M $HAuCl_4$(aq.) obtained at 200 μL, and the variations of $n_{(HAuCl4/NaBH4)}$ are **d** 2:1, **e** 1:5, and **f** 1:10

wavelength range. With Au nanocrystals inside, the $Au@SiO_2$ hybrid nanoparticles exhibit a well-defined absorption peak between 480 and 600 nm. When the volume of $HAuCl_4$ is 50 μL, it produces a plasmon resonance peak (λ_{max}) at 530 nm. With the increase of the addition amount of $HAuCl_4$ (100 μL), the plasmon resonance band broadens, displays a red shift ($\lambda_{max}=535$ nm), and decreases in intensity, indicating the formation of gold nanoparticle dimmers as can be observed in the TEM images. When 270 μL $HAuCl_4$ is added to the microemulsion, the UV absorption curve becomes very broad and the maximum shifts to 549 nm with a very low intensity. That is caused by the formation of larger gold nanoparticle assemblies [33].

In addition, to investigate the thermal stability of the particles for other potential applications such as catalyst supports, TGA of $Au@SiO_2$ nanoparticles was carried out in comparison to pure SiO_2 nanoparticles (Fig. 3b). It is found that the weight loss of pure SiO_2 nanoparticles is only 6.3 %, and the weight losses of $Au@SiO_2$ nanoparticles at 100 and 200 μL $HAuCl_4$ are 12.4 and 13.8 % up to 800 °C, respectively, demonstrating excellent thermal stability of the $Au@SiO_2$ hybrid nanoparticles due to the coated SiO_2 protecting layer.

Detailed characterization of $Au@SiO_2$ hybrid nanoparticles

Figure 4 gives a typical result of $Au@SiO_2$ hybrid nanoparticles synthesized at $n_{(HAuCl4/NaBH4)}=1$, and the volume of $HAuCl_4$ is 200 μL. It can be seen that the average diameter of the Au nanodots within the silica matrix was 4.84±0.62 nm (more than 100 silica NPs were evaluated) as shown in Fig. 4a. HR-TEM images show that each individual Au

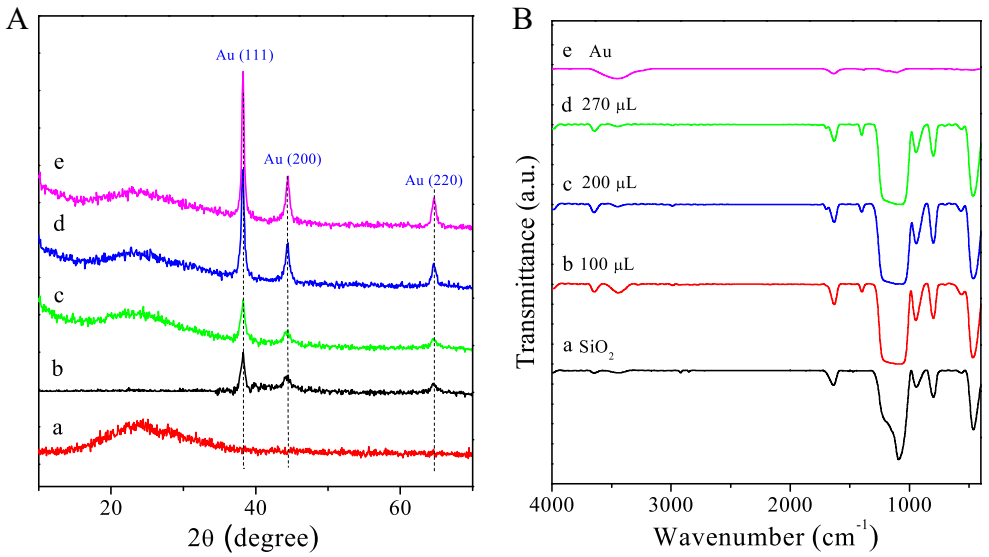

Fig. 2 **a** XRD patterns of SiO_2 nanoparticles (*a*) and XRD results (*b*) of the bare Au nanocrystals obtained after removal the outer SiO_2 layer of the Au@SiO_2 hybrid nanoparticles by NaOH etching. XRD patterns of Au@SiO_2 hybrid nanoparticles synthesized using 0.2 M $HAuCl_4$(aq.) obtained at $n_{(HAuCl4/NaBH4)}$=1 and the variations of the volume of $HAuCl_4$ are 100 μL (*c*), 200 μL (*d*), and 270 μL (*e*). **b** FTIR spectra of (*a*) SiO_2 nanoparticles and Au@SiO_2 hybrid nanoparticles synthesized at synthesized using 0.2 M $HAuCl_4$(aq.) obtained at $n_{(HAuCl4/NaBH4)}$=1 and the variations of the volume of $HAuCl_4$ are 100 μL (*b*), 200 μL (*c*), 270 μL (*d*), and bare (*e*) Au nanocrystals after removal the outer SiO_2 layer of the Au@SiO_2 hybrid nanoparticles by NaOH etching, respectively

nanodot is a single crystal, and the observed lattice-fringe distances of 0.235 nm are assigned to the spacings between the (111) lattice planes in the crystalline fcc structures of gold (Fig. 4b) [4]. Figure 4c is the selected area electron diffraction (SAED) pattern of Au nanodots. Elemental analysis by energy-dispersive X-ray spectroscopy (EDX) analysis prove that nanoparticles with an Au component are present within the silica (SiO_2) matrix (Fig. 4d).

A classical XPS characterization was conducted to corroborate the previous TEM observations and to determine the chemical environments in the Au@SiO_2 structure. Figure 5 shows the XPS survey spectrum of Au@SiO_2 hybrid nanoparticles synthesized at $n_{(HAuCl4/NaBH4)}$=1, and the volume of $HAuCl_4$ is 200 μL. Signals from Au 4f, Si 2p, and O 1 s can be clearly observed (Fig. 5a), indicating the chemical composition of the Au@SiO_2 hybrid nanoparticle. From the magnified spectrum, it can be seen that the Au 4f signal consists of two adjacent peaks assigned to be Au 4f 5/2 (BE=85.1 eV) and Au 4f 7/2 (BE=88.2 eV), respectively (Fig. 5b) [34] and peaks representing Au 4d locates at BE=364.8 eV [35]. Peaks representing Si 2p and O 1 s locate at BE=103.6 eV (Fig. 5c) and 528.0 eV (Fig. 5d), respectively.

In view of these results, although the silica shell was considered to be mesoporously structured [36], its thickness was definitively more than the XPS sampling depth (TEM showed a 20-nm-thick SiO_2 layer around Au/ core). These XPS results point out the limitations of XPS spectroscopy for the analysis of such core–shell nanoparticles [34].

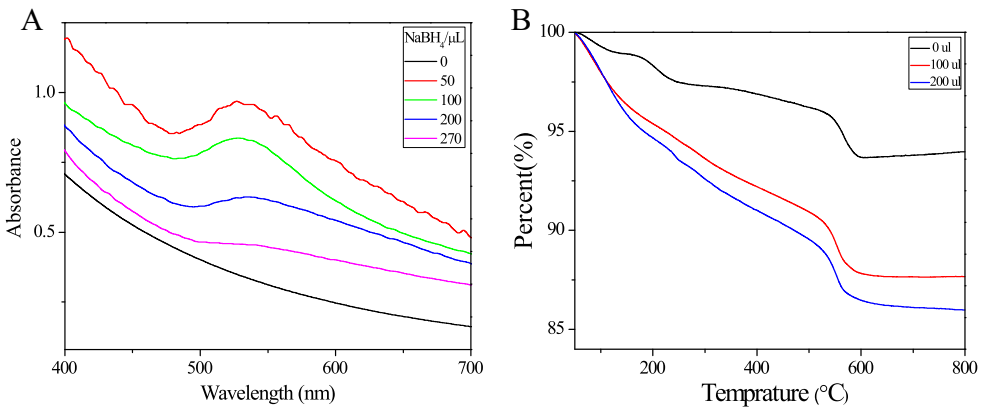

Fig. 3 UV absorption of SiO_2 nanoparticles and Au@SiO_2 hybrid nanoparticles synthesized using 0.2 M $HAuCl_4$(aq.) obtained at $n_{(HAuCl4/NaBH4)}$=1 and different volumes of $HAuCl_4$. TGA curves of pure SiO_2 nanoparticles and different structures of Au@SiO_2 nanoparticles synthesized using 0.2 M $HAuCl_4$(aq.) obtained at $n_{(HAuCl4/NaBH4)}$=1 and different volumes of $HAuCl_4$

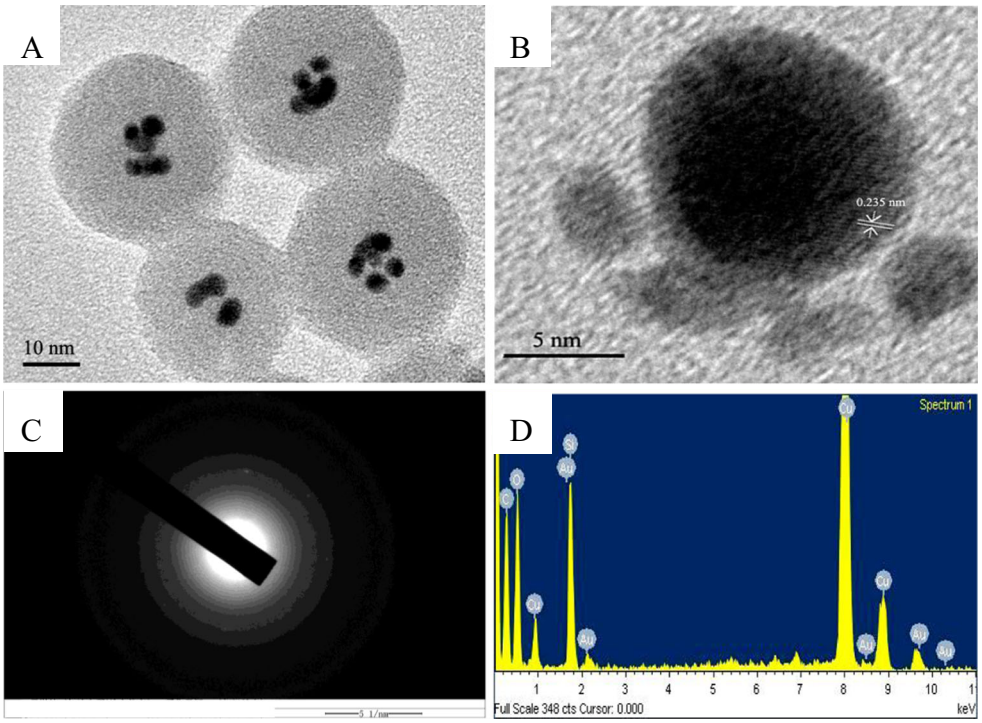

Fig. 4 TEM (**a**, amplification of Fig. 1c) and HR-TEM (**b**) images of $Au@SiO_2$ hybrid nanoparticles synthesized at $n_{(HAuCl4/NaBH4)}=1$ and the volume of $HAuCl_4$ is 200 μL. **c** The selected area electron diffraction (SAED) pattern and **d** the EDS result

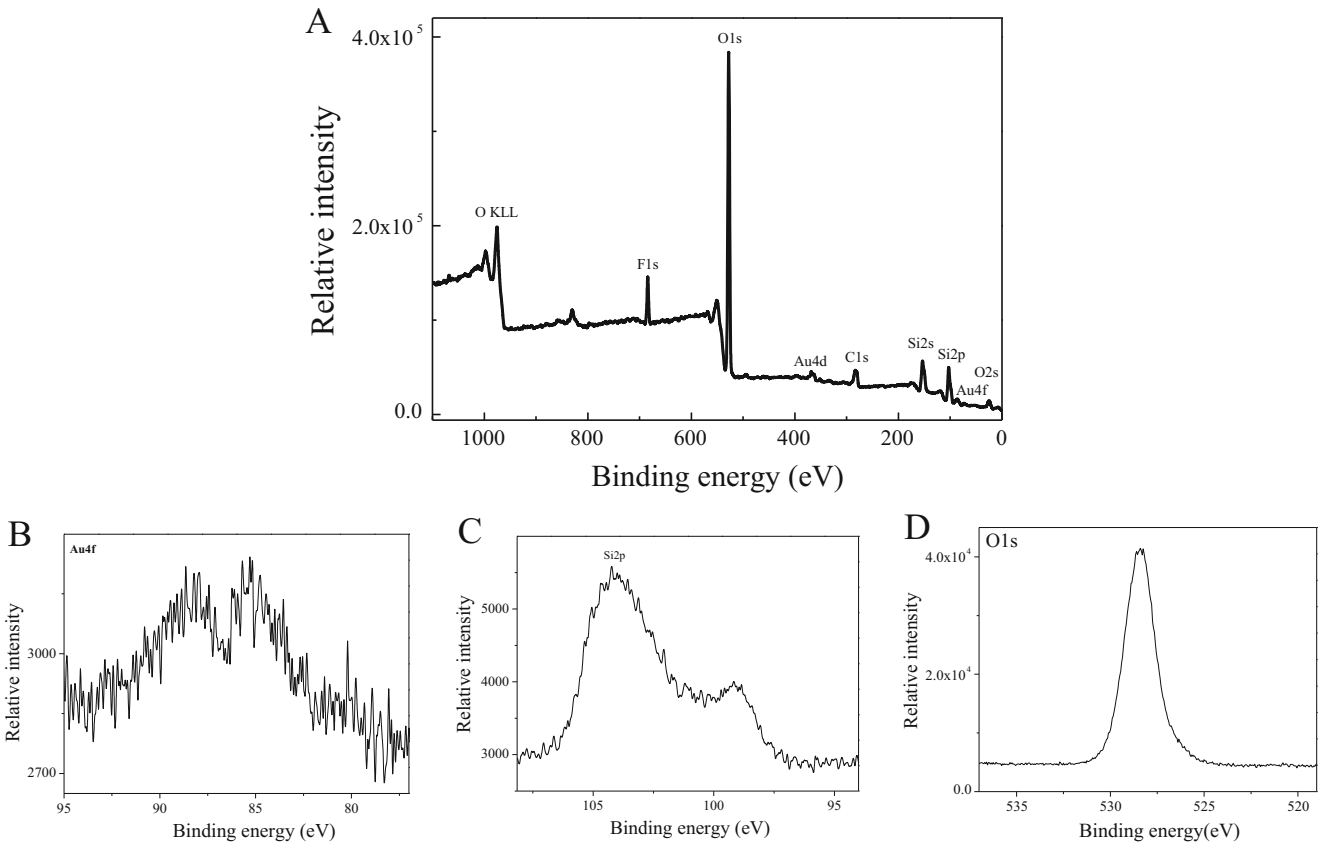

Fig. 5 XPS survey spectrum of $Au@SiO_2$ hybrid nanoparticles synthesized at $n_{(HAuCl4/NaBH4)}=1$ and the volume of $HAuCl_4$ is 200 μL. **a** The overall spectrum and (**b**–**d**) magnified spectra of Au 4f, Si 2p, and O 1 s

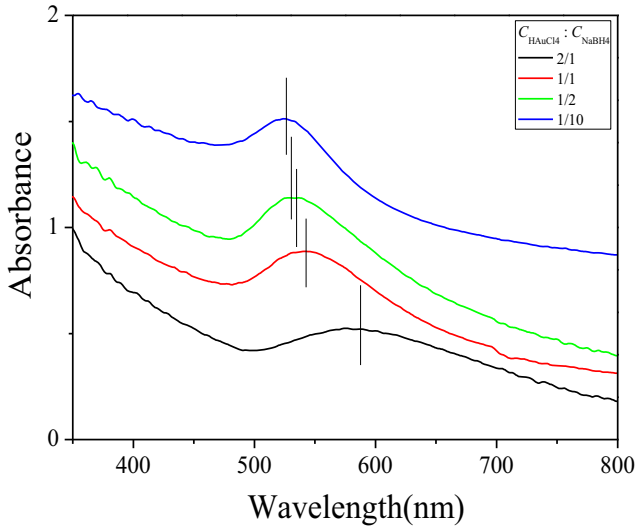

Fig. 6 UV-vis absorption of $Au@SiO_2$ NPs that were synthesized using 0.2 M $HAuCl_4$(aq.) obtained at 200 μL with the variations of $n_{(HAuCl4/NaBH4)}$

The morphology of $Au@SiO_2$ nanoparticles with the variations of $n_{(HAuCl4/NaBH4)}$

Besides considering the variations of the volume of $HAuCl_4$ on the influence of the morphology of $Au@SiO_2$ nanoparticles, we also investigated the variations of $n_{(HAuCl4/NaBH4)}$ on the morphology of them. TEM images of $Au@SiO_2$ NPs that were synthesized using 0.2 M $HAuCl_4$(aq.) obtained at 200 μL with the variations of $n_{(HAuCl4/NaBH4)}$ are shown in Fig. 6. It can be seen that when $n_{(HAuCl4/NaBH4)}$=2 (Fig. 1d), the Au nanodots in the core are individual, but with the decrease of $n_{(HAuCl4/NaBH4)}$, the Au nanodots in the core–shell structure become scattered (Fig. 1c, e). When $n_{(HAuCl4/NaBH4)}$=0.1, the Au nanodots again aggregate into a single solid (Fig. 1f). Moreover, with the decrease of $n_{(HAuCl4/NaBH4)}$, the cavities in the core–shell structure increase and become larger and when $n_{(HAuCl4/NaBH4)}$=0.1, the hollow cavities become smaller again. It is speculated that when $n_{(HAuCl4/NaBH4)}$ is small which is at 2, the reduction reaction occurs slowly and it releases less

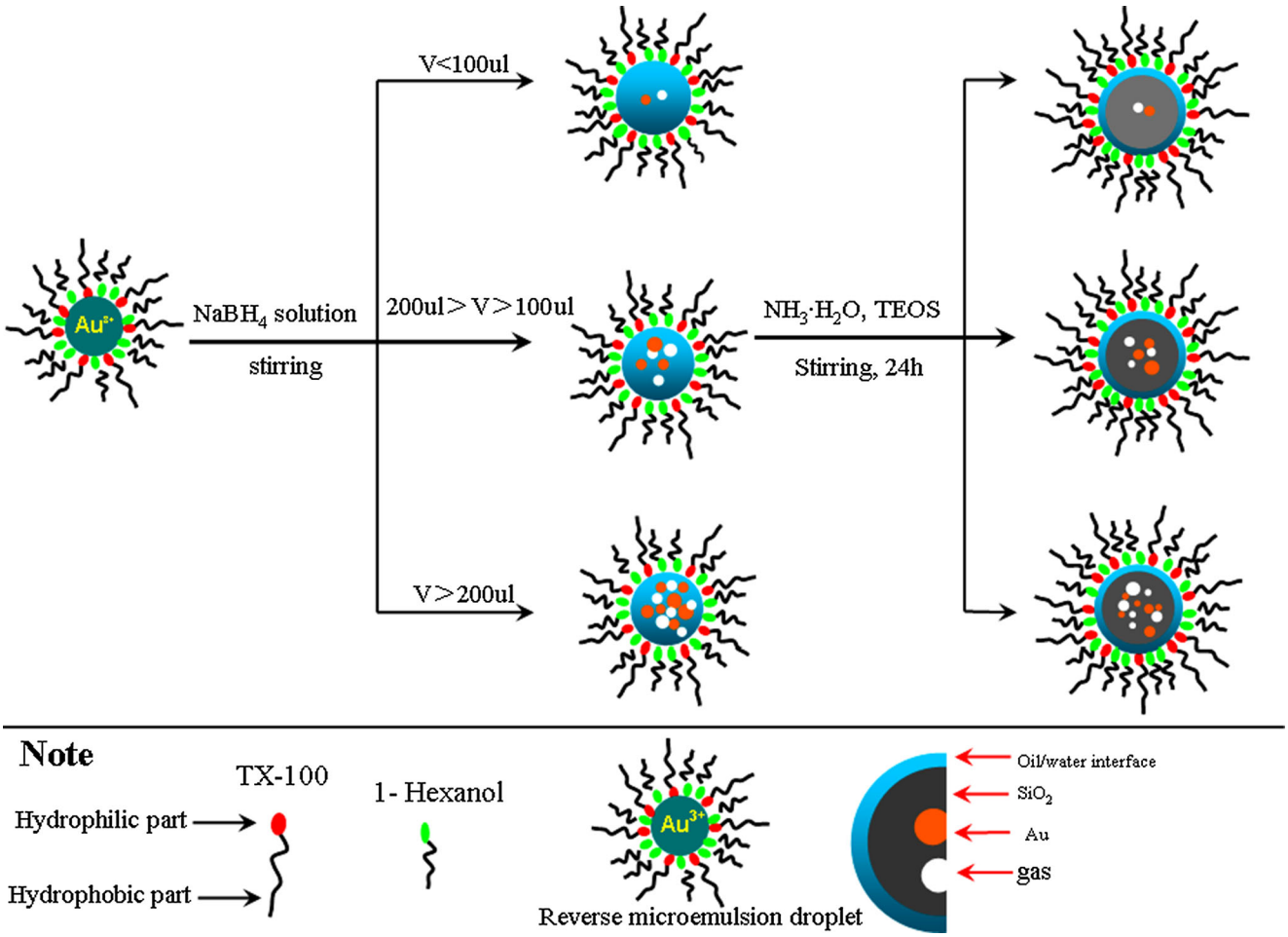

Scheme 2 Schematic illustration of the formation mechanism of $Au@SiO_2$ hybrid nanoparticles with the variations of the volume of 0.2 M $HAuCl_4$ in the Triton X-100/1-hexanol/cyclohexane/H_2O water-in-oil microemulsions

gas, the restored gold can be aggregated into small solid nanodots in the mild environment. When $n_{(HAuCl4/NaBH4)}$ decreases form 1 to 0.5, the reduction reaction becomes more intense and it releases more gas quickly and they wrap in SiO_2 shell to slowly spread which can induce the formation of larger cavities (inset of Fig. 1e). However, it is also because of the quick reaction, the restored gold has no time to polymerized into a solid sphere but only exists in small dots. When $n_{(HAuCl4/NaBH4)}$ further decrease to 0.1, the reaction is too intense and the release of the gas basically escaped in one moment before SiO_2 starting to form the shell; thus, there are less cavities or no cavity in the SiO_2 shell. After the escape of gas, the reduced gold can gradually aggregate into a larger solid center in a relatively calm environment.

Figure 6 shows the UV-vis absorption of Au@SiO_2 NPs that were synthesized using 0.2 M $HAuCl_4$(aq.) obtained at 200 μL with the variations of $n_{(HAuCl4/NaBH4)}$. It can be seen that with the decrease of $n_{(HAuCl4/NaBH4)}$, the plasmon resonance band becomes more and more narrow and displays a blue shift (from λ_{max}=587 nm at $n_{(HAuCl4/NaBH4)}$=2 to λ_{max}= 526 nm at $n_{(HAuCl4/NaBH4)}$=0.1), indicating the formation of more and more monodispersed gold nanoparticles as can be observed in the TEM images.

Formation mechanism of Au@SiO_2 hybrid nanoparticles

According to the experimental results above, the plausible mechanism of the formation of Au@SiO_2 hybrid nanoparticles with the variations of the volume of $HAuCl_4$ is schematically shown in Scheme 2. It can be seen that both the size of Au@SiO_2 hybrid nanoparticles and the number of Au nanodots encapsulated in the SiO_2 shell could be successfully controlled by varying the volume of $HAuCl_4$. That is to say that the number of Au nanodots encapsulated within the silica shell could be effectively controlled by changing the addition amount of $HAuCl_4$ and the water to surfactant ratio.

Conclusions

Different structures of Au@SiO_2 hybrid nanoparticles have been successfully synthesized using a Triton X-100/1-hexanol/cyclohexane/H_2O water-in-oil microemulsion as a soft template. Typically, the nanoparticle has a SiO_2 protecting layer containing Au nanocrystals inside. By changing the volume of $HAuCl_4$ and $n_{(HAuCl4/NaBH4)}$, we can get single solid Au core or multiple Au nanodots in the SiO_2 shell. Cavities induced by H_2 gas production during Au^{3+} reduction could be observed if the reduction reaction becomes so intense which releases the H_2 gas quickly and induces H_2 gas wrapped in SiO_2 shell to slowly spread. It is believed that the unique properties exhibited by the nanoparticles comprising single and multiple Au nanodots together with cavities can be further tuned and expanded their applications to various areas, including catalysis, surface-enhanced Raman scattering (SERS) detection, biology, and medicine.

Acknowledgments We gratefully acknowledge financial support from the National Natural Science Foundation of China (21203109) and Ji'nan Youth Science and Technology Star Program (2013040).

References

1. El-Sayed MA (2001) Acc Chem Res 34:257
2. Xia Y, Xiong Y, Lim B, Skrabalak SE (2009) Angew Chem Int Ed 48:60
3. Hu M, Chen J, Li ZY, Au L, Hartland GV, Li X, Marquez M, Xia Y (2006) Chem Soc Rev 35:1084
4. Pak J, Yoo HJ (2013) J Mater Chem A 1:5408
5. Daniel MC, Astruc D (2004) Chem Rev 104:293
6. Ghosh SK, Pal T (2007) Chem Rev 107:4797
7. Takenaka S, Hirata A, Tanabe E, Matsune H, Kishida M (2010) J Catal 274:228
8. Zhou C, Peng F, Wang H, Yu H, Peng C, Yang J (2010) Electrochem Commun 12:1210
9. Yeung CMY, Tsang SC (2009) J Phys Chem C 113:60
10. Maeda K, Sakamoto N, Ikeda T, Ohtsuka H, Xiong A, Lu D, Kanehara M, Teraishi T, Domen K (2010) Chem Eur J 16:7750
11. Fan H, Yang K, Boye DM, Sigmon T, Malloy KJ, Xu H, López GP, Brinker CJ (2004) Science 304:567
12. Avnir D, Coradin T, Lev O, Livage J (2006) J Mater Chem 16:1013
13. Han Y, Jiang J, Lee SS, Ying JY (2008) Langmuir 24:5842
14. Mahtab F, Yu Y, Lam JWY, Liu J, Zhang B, Lu P, Zhang X, Tang BZ (2011) Adv Funct Mater 21:1733
15. Jing L, Yang C, Qiao R, Niu M, Du M, Wang D, Gao M (2010) Chem Mater 22:420
16. Qi G, Wang Y, Estevez L, Switzer AK, Duan X, Yang X, Giannelis EP (2010) Chem Mater 22:2693
17. Hong J, Lee J, Rhymb YM, Kim DH, Shim SE (2010) J Colloid Interface Sci 344:410
18. Wong YJ, Zhu LF, Teo WS, Tan YW, Yang YH, Wang C, Chen HY (2011) J Am Chem Soc 133:11422
19. Zhu LF, Wang H, Shen XS, Chen LY, Wang YW, Chen HY (2012) Small 8:1857
20. Liz-Marzán LM, Mulvaney P (2003) J Phys Chem B 107:7312
21. Lu Y, Yin Y, Li ZY, Xia Y (2002) Nano Lett 2:785
22. Yin Y, Lu Y, Sun Y, Xia Y (2002) Nano Lett 2:427
23. Graf C, Vossen DLJ, Imhof A, van Blaaderen A (2003) Langmuir 19: 6693
24. Kobayashi Y, Katakami H, Mine E, Nagao D, Konno M, Liz-Marzán LM (2005) J Colloid Interface Sci 283:392
25. Lu H, Ju HF, Yang Q, Li ZR, Ren HY, Xin X, Xu GY (2013) Cryst Eng Comm 15:6511
26. Guo HX, Zhao XP, Guo HL, Zhao Q (2003) Langmuir 19:9799
27. Jongsomjit B, Kittiruangrayub S, Praserthdam P (2007) Mater Chem Phys 105:14
28. Xiao JY, Qi LM (2011) Nanoscale 3:1383
29. Lin J, Siddiqui JA, Ottenbrite RM (2001) Polym Adv Technol 12:285
30. Link S, El-Sayed MA (1999) J Phys Chem B 103:8410
31. Kreibig U, Vollmer W (1995) Optical Properties of Metal Clusters, Springer Series in Materials Science. Springer, Berlin

32. Link S, El Sayed MA (2000) Int Rev Phys Chem 19:409
33. Wang H, Schaefer K, Moeller M (2008) J Phys Chem C 112:3175
34. Ledeuil JB, Uhart A, Soulé S, Allouche J, Dupin JC, Martinez H (2014) Nanoscale 6:11130
35. Pârvulescu VI, Pârvulescu V, Endruschat U, Filoti G, Wagner FE, Kübel C, Richards R (2006) Chem Eur J 12:2343
36. Soulé S, Allouche J, Dupin JC, Martinez H (2013) Microporous Mesoporous Mater 171:72